RSC Advances

ROYAL SOCIETY OF CHEMISTRY

www.rsc.org/advances

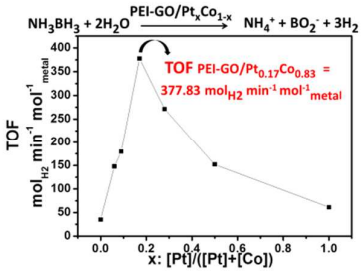

PEI-GO/$Pt_{0.17}Co_{0.83}$ was synthesized and showed the best catalytic activity among the reported Pt-based bimetallic catalysts for hydrolysis of ammonia borane.

RSC Advances

RSCPublishing

ARTICLE

A High-Performance Pt-Co Bimetallic Catalyst with Polyethyleneimine Decorated Graphene Oxide as Support for Hydrolysis of Ammonia Borane

Mengxiong Li [a†], Jiantong Hu [a†], Zhongxin Chen [a] and Hongbin Lu* [a]

Cite this: DOI: 10.1039/x0xx00000x

Received XXth June 2014,
Accepted XXth XXX 2014

DOI: 10.1039/x0xx00000x

www.rsc.org/

A series of Pt_xCo_{1-x} bimetallic nanoparticles (NPs) were deposited on polyethyleneimine (PEI)-decorated graphene oxide (GO) by a simple co-reduction method. The PEI molecules facilitated the uniform distribution of bimetallic NPs (~ 2.3 nm) on GO. Among these catalysts, PEI-GO/$Pt_{0.17}Co_{0.83}$ showed extraordinary catalytic properties, a total turnover frequency (TOF) of 377.83 mol_{H2} min^{-1} mol^{-1}_{metal}, a hydrogen generation rate of 111.28 L_{H2} min^{-1} g^{-1}_{metal} at 298K, an activation energy of 51.6 kJ mol^{-1} and good recyclability (~ 80% after 5 cycles). The synergistic effect between Pt and Co, and small sizes of NPs play important roles in improving their catalytic properties. Such low-cost, recyclable bimetallic catalysts enable many practical applications in portable devices and fuel cells.

Introduction

Hydrogen is a clean, effective energy carrier that meets the increasing energy demands and can be used in fuel cells and portable devices,[1-3] which requires high hydrogen capacity materials and high real-time production efficiency, and thus spurs strong interest in recent years.[4-6] Ammonia borane (NH_3BH_3, AB) is one of the most promising chemical hydrogen storage materials, with many advantages, *e.g.*, low molecular weight, high hydrogen capacity (19.6 wt%), nontoxicity, high water solubility and chemical stability.[7,8] Compared with the thermolysis, hydrolysis of AB can be completed at lower reaction temperatures and reveals higher dehydrogenation rates.[9] Also, it can release sustained amount of hydrogen when proper catalysts are employed.[10] This makes performance optimization of catalysts a critical prerequisite for improving dehydrogenation efficiency of AB hydrolysis.

Noble metals[11,12] and non-noble metals[13-15] have long been studied for the catalytic hydrolysis of AB. However, noble metal catalysts usually suffer from resource and cost limitations while non-noble metal catalysts only have moderate activity and stability. Compared to monometallic catalysts, much better selectivity and catalytic activity of bimetallic catalysts have recently been demonstrated.[16,17] In bimetallic systems two effects are found to play important roles. The first one is the geometric effect, in which the coordination of one metal to another provides new active sites. The other is the electronic effect, that is, the addition of one metal alters the electron properties of another metal due to the electron transfer. It is difficult to distinguish these two effects, instead both are called the synergistic effect between two metals.[18] Owing to such synergistic effect, bimetallic catalysts can show significantly improved catalytic activity even at lower concentrations than monometallic catalysts.[19] To optimize their performance, morphology control of bimetallic NPs is important, different structures such as core-shell structure, heterostructure and alloy structure have been designed to make the best of bimetallic synergistic effect. On the other hand, the form of bimetallic systems also improves the stability of catalysts. For example, Jiang et al.[20] synthesized Au-Ni@SiO_2 catalysts that revealed better catalytic activities than corresponding monometallic catalysts. Wen et al.[21] prepared hexagonal NiCo-Pt nanoplate catalysts to achieve remarkably improved catalytic activities. Xu et al.[22] demonstrated that improved catalytic activity and recyclability of PdPt cubic NPs. These bimetallic catalysts with controlled composition, size and morphology provide a desired solution for practical applications of AB hydrolysis.

Nevertheless, it must be considered that small bimetallic NPs have high specific surface areas (SSA), which causes a strong particle aggregation propensity. To optimize their catalytic activity and recyclability, employment of suitable support is necessary for preventing aggregation and maximizing their SSA and catalytic activity. Graphene, a 2-dimensiaonl carbon films with single-atom thickness, has emerged as a promising candidate owing to its high SSA and extraordinary properties.[23,24] Also, it may interact directly with metal NPs to enhance the electron transfer efficiency and catalytic activity.[25] So far, there have been many studies that were dedicated to developing graphene-based catalysis.[26,27] However, the size and spatial distributions of resulting metal NPs on graphene are often not well-controlled.[28] To conquer this shortcoming, various organic functional polymers have been used to tune the morphology and spatial distribution of metal NPs deposited on graphene. The functional groups of the polymers can

immobilize metal ions, leading to the well dispersion of metal NPs after reduction.[29,30] In our previous study,[31] branched polyethylene-imine (PEI) has been found to be valid in morphology optimization and performance enhancement of metal NPs deposited on graphene oxide (GO), which greatly helps increase the catalytic activity of the catalyst.

In this work we make full use of synergistic effect between Pt and Co and uniform dispersion of small-sized metal NPs on PEI-decorated GO to significantly improve catalytic activity and stability of catalysts. We synthesize a series of Pt_xCo_{1-x} bimetallic NPs that are deposited on PEI-GO and examine their catalytic activity and recyclability for AB dehydrogenation. We find that their catalytic performance shows a volcano-shape relationship with changing Pt/Co ratios. When the Pt/Co ratio in composite catalysts reaches 0.2, that is, PEI-GO/$Pt_{0.17}Co_{0.83}$, a catalytic activity that is superior to all reported other Pt-based bimetallic catalysts is observed, exhibiting a TOF value of 377.83 mol_{H2} min^{-1} mol^{-1}_{metal}, a maximum hydrogen generation rate of 111.28 L_{H2} min^{-1} g^{-1}_{metal} at room temperature and good recyclability, capable for further applications in fuel cells and portable devices.

Experimental Section

Chemicals

Graphite powder 8099200 (120 μm) was purchased from Qingdao BCSM Co. 98% H_2SO_4, 65% HNO_3, 30% H_2O_2, 96.0% sodium borohydride and 98% $H_2PtCl_6{\cdot}6H_2O$ were obtained from Sinopharm Chemical Regent Co., sodium nitrate came from Shanghai Qiangshun Chemical Co., $KMnO_4$ was from Shanghai Zhenxin Chemical Co., polyethyleneimine (PEI, M_w = 600, branched) and cobalt (II) acetate tetrahydrate were purchased from Alfa Aesar, ammonia-borane complex (97%) was from Aldrich. All chemicals were used as received. Deionized water (DI water) was used in all experiments.

Characterization

Transmission electron microscopy (TEM, JEM-2100F and Tecnai G^2 20 Twin, both operating at 200 kV) was used to observe the morphology of PEI-GO/Pt_xCo_{1-x} at different magnifications. All samples for imaging were prepared by depositing aqueous dispersions (~0.2 mg mL^{-1}) on holey copper grids. Fourier transform infrared spectroscopy (FT-IR) was recorded on a NEXUS 670 spectrometer at room temperature over a frequency range of 3750 - 750 cm^{-1}. Thermogravimetric analysis (TGA) was conducted with Pyris 1 TGA and nitrogen as a purge gas, from ambient temperature to 800 °C at a heating rate of 20 °C min^{-1}. X-ray photoelectron spectra (XPS) were carried out on an AXIS UltraDLD system (Kratos) with monochromatic Al K_α radiation (hv = 1486.6 eV). X-ray diffraction (XRD) tests were carried out using PANalytical X'Pert PRO X-ray diffractometer with Cu K_α radiation (λ = 1.54 Å) at a scanning rate of 14º min^{-1} in 2θ range from 30 to 80º.

Preparation of the Catalysts

GO was prepared by the Hummers method and freeze-dried before use. Then GO (50 mg) was dissolved in DI water (10 mL) with ultrasonication and DI water (10 mL) containing PEI (1 g) was slowly added. The mixture was stirred magnetically at 60 °C for 24 h to synthesize PEI-GO. After that, the mixture was purified by centrifugation and freeze-dried to constant weight. PEI-GO supported catalysts were prepared by the deposition of metal NPs on support. Typically, as-prepared PEI-GO (0.5 mg) was dissolved in DI water (10 mL) with ultrasonication in a two necked round-bottom flask. $Co(Ac)_2{\cdot}4H_2O$ (2.5 μmol) and $H_2PtCl_6{\cdot}6H_2O$ (0.5 μmol) were added to the above solution. The mixture was stirred for 15 min under N_2 atmosphere. Then $NaBH_4$ (5 mg) was added into the mixture to synthesize PEI-GO/$Pt_{0.17}Co_{0.83}$ catalyst. The collected product was washed with DI water, ethanol and dried in a two-necked flask under the protection of nitrogen atmosphere.

For better comparison, we fixed the usage of $H_2PtCl_6{\cdot}6H_2O$ in all experiments, while changing the usage of $Co(Ac)_2{\cdot}4H_2O$ according to the normalized Pt/Co ratios at 1:1, 1:2.5, 1:5, 1:10 and 1:15. We also fixed the ratio of PEI-GO to metal precursors (0.5 mg PEI-GO to 3 μmol metal precursors) to avoid possible influence on the deposition of NPs. This leaded to PEI-GO/$Pt_{0.5}Co_{0.5}$, PEI-GO/$Pt_{0.29}Co_{0.71}$, PEI-GO/$Pt_{0.17}Co_{0.83}$, PEI-GO/$Pt_{0.09}Co_{0.91}$ and PEI-GO/$Pt_{0.06}Co_{0.94}$ catalysts. We also prepared monometallic PEI-GO/Pt and PEI-GO/Co by the same method, except for a higher usage of metal precursor (10 μmol for Pt and 50 μmol for Co).

Catalytic Hydrolysis of AB

The as-prepared PEI-GO/Pt_xCo_{1-x} was dispersed into 8 mL aqueous solution in a two-necked round-bottom flask. AB (1.1 mmol) dissolved in DI water (2 mL) was injected into the solution with a syringe under stirring (1200 rpm). The reaction was carried out under ambient condition. The volume of the H_2 generated was monitored with a gas burette. To study the effect of reaction temperature, we performed the test at four different temperatures (15, 25, 35 and 45 °C) for the dehydrogenation of AB.

Recycle Tests of the Catalysts

After the dehydrogenation reaction was completed, the catalyst was collected at the bottom of the flask with a magnet and supernatant was carefully removed. After being washed, DI water (8 mL) was added to the flask and then DI water (2 mL) containing AB (1.1 mmol) was injected into the solution for recycle tests. The same process was repeated for 5 times.

Results and Discussions

The PEI-GO support was prepared by a modified method from our previous work.[31] In brief, GO was first dispersed in water followed by dropping desired amounts of PEI (M_w = 600) aqueous solution. After stirring for 24 h at 60 °C, the color of the suspension changes from brown to dark grey, indicating a partial reduction of GO.[32] A large amount of amine groups on branched PEI enable them to be adsorbed or covalently linked to GO. Due to the presence of carboxyl groups, GO can bind with positively charged PEI molecules by the electrostatic interaction with amine groups and the formation of amide bonds.[33]

As shown in **Fig. 1a**, GO has a sharp weight loss around 200 °C, which is attributed to thermal removal of adsorbed water and part of oxygen-containing groups. For PEI, its main weight loss stage between 300 ~ 400 °C stems from the decomposition of polymer skeleton. By comparison, PEI-GO has a weight loss of about 40% in this range; we thus speculate that a significant amount of PEI (~ 40%) has been deposited on GO. In **Fig. 1b**, a small shoulder around 1660 cm^{-1} would originate from amide bonds of PEI-GO, suggesting that part of

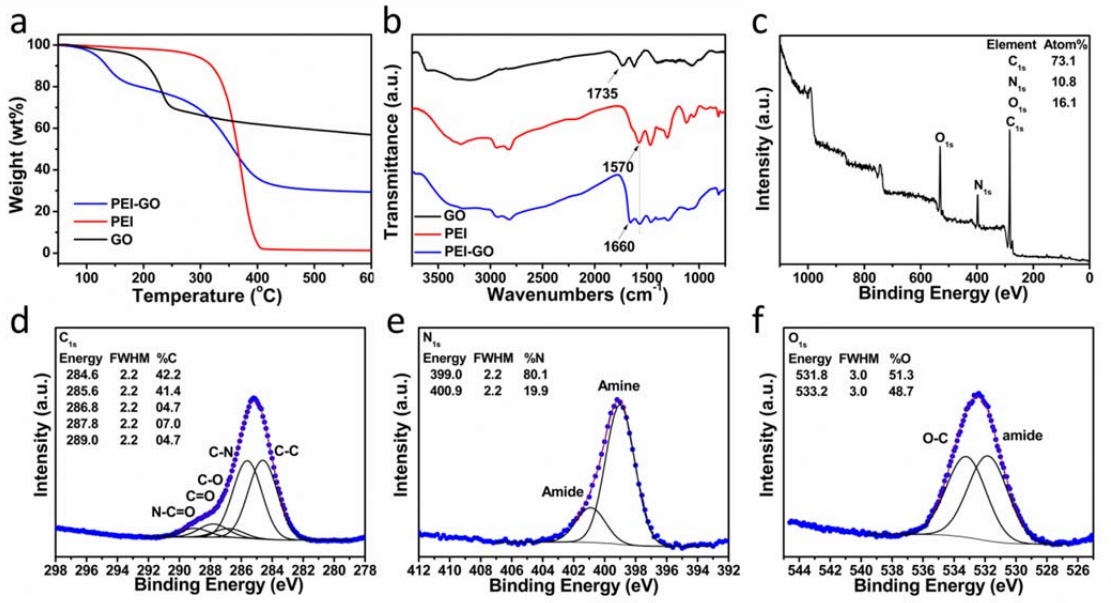

Fig. 1 (a) TGA curves and (b) FT-IR spectra of GO, PEI and PEI-GO composite; XPS spectra of (c) PEI-GO and the corresponding (d) C_{1s}, (e) N_{1s} and (f) O_{1s} core-levels for PEI-GO.

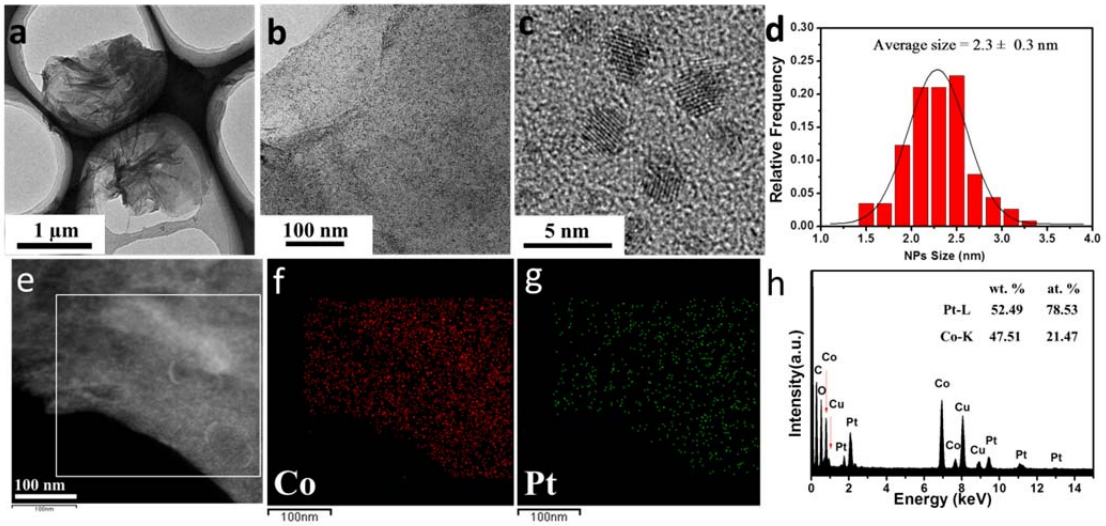

Fig. 2 Microscopy investigation of PEI-GO/$Pt_{0.17}Co_{0.83}$. (a, b) TEM and (c)HRTEM images at different magnifications; (d) size distribution for metal NPs; (e-h) STEM dark field image, elemental mapping images and corresponding EDX spectrum.

PEI molecules form covalent linkage with GO. XPS survey of PEI-GO composite was utilized to identify the chemical composition of PEI-GO. In **Fig. 1d** the C_{1s} core-level is fitted with five Gaussian peaks at 284.6, 285.6, 286.8, 287.8 and 289.0 eV, which can be ascribed to C-C, C-N, C-O, C=O and N-C=O species, respectively. The existence of N-C=O species means that PEI molecules are confined by GO through covalent bonding interaction. It is seen that the C-N species are the major functional groups (41.4%) due to the deposition of PEI molecules after reaction. This is in accord with the N_{1s} spectrum in **Fig. 1e**, where ~ 80.0% amine groups (at 399.0 eV) are observed for PEI-GO. This enables the coordination interaction between metal ions and amine groups, so that most of the NPs could be confined within the polymer framework during the sequent fast reduction, and result in the uniform distribution of NPs on PEI-GO.

Subsequently, we observe the morphology of the as-prepared PEI-GO/$Pt_{0.17}Co_{0.83}$ with TEM. **Fig. 2a** shows the microscopic structure of PEI-GO/$Pt_{0.17}Co_{0.83}$ where obvious folds and corrugations are visible, indicating the coverage of PEI on GO surface.[31] **Fig. 2b** displays numerous dark Pt and Co NPs that have been deposited on PEI-GO. They are all distributed compactly, which help to prevent the aggregation of graphene nanosheets. **Fig. 2c** clearly shows the sizes of metal NPs. We calculated the size distribution of metal NPs from at least 100 NPs, which is shown in **Fig. 2d**. Since most metal ions are strongly restricted within the PEI layers (heterogeneous nucleation effect), homogeneous nucleation in the bulk solution is hard to take place, which results in formation of small metal

NPs (~ 2.3 nm). The uniform dispersion of Pt and Co NPs on PEI-GO is also confirmed by the STEM dark field image in **Fig. 2e**. Since Co (Z = 27) and Pt (Z = 78) have a much higher contrast than those low Z-number elements such as C, O, N, the bright spots in dark field image reflect the location of metal NPs on PEI-GO. The corresponding elemental mapping images are shown in **Fig. 2f** and **2g**, where the red spots represent Co NPs and green spots Pt NPs. The ratio of Pt to Co is calculated as ~ 1:4 according to **Fig. 2h**, which is close to the feed ratio (1:5). This is consistent with the speedy nucleation and growth process of metal NPs (< 10 s) under a strong reductant with the help of the support. These results make us conclude that Pt and Co are well dispersed in the PEI-GO/$Pt_{0.17}Co_{0.83}$, and expect an improved performance for catalytic hydrolysis of AB at room atmosphere. XRD patterns of PEI-GO/Pt_xCo_{1-x} with different x values are shown in **Fig. S1**. There are no obvious peaks appear during the 2θ range from 30 to 80º, indicating the amorphous structure of metal NPs.

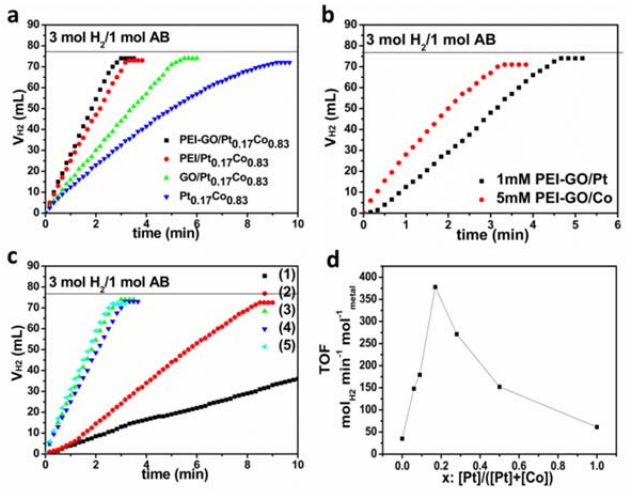

Fig. 3 Hydrogen generation from AB with different catalysts at 25 ± 0.5 °C: (a) $Pt_{0.17}Co_{0.83}$, *GO/*$Pt_{0.17}Co_{0.83}$*, PEI/*$Pt_{0.17}Co_{0.83}$ and PEI-GO/$Pt_{0.17}Co_{0.83}$. (b)PEI-GO/Pt and PEI-GO/Co. (c) PEI-GO/Pt_xCo_{1-x} with (1) x = 0.5; (2) x = 0.29; (3) x = 0.17; (4) x = 0.09, and (5) x = 0.06 and (d) the corresponding plots of TOF *versus* x (x = 1, 0.5, 0.29, 0.17, 0.09, 0.06 and 0) for PEI-GO/Pt_xCo_{1-x}. [AB] = 110 mM. For monometallic PEI-GO/Pt and PEI-GO/Co, [Pt] = 1 mM and [Co] = 5 mM; while for bimetallic catalysts, [Pt] = 0.05 mM. [Co] is calculated from the normalized Pt/Co ratios. Volume of the dispersion is 10 mL.

Table. 1. Comparison of catalytic activity and activation energy of various noble metal-based bimetallic catalysts for the hydrolysis of AB.

Catalysts	TOF[a] mol_{H2} min^{-1} mol^{-1}_{metal}	Activation energy kJ mol^{-1}	Ref.
PEI-GO/$Pt_{0.17}Co_{0.83}$	377.83	51.6	This study
$Ni_{0.33}$@$Pt_{0.67}$/C	166.91	33.0	34
$Co_{0.32}$@$Pt_{0.68}$/C	147.63	41.5	35
PdPt cubic NPs	50.02	21.8	22
Pt /CeO_2/RGO	48	-	36
Ru@Ni/graphene	45.27	36.6	25
Pd@Co/graphene	37.44	-	37
$Ni_{16}Co_{80}/Pt_4$	30.77	45.7	38
$Pt_{0.65}Ni_{0.35}$	28.82	39	39
$Co_{35}Pd_{65}$/C	22.7	27.5	19
RuCo/γ-Al_2O_3	12.69	52	40
Pt/γ-Al_2O_3	222.22	21	41
Pt-MIL	211.27	40.7	42

[a] For core-shell structure, only the shell metals are taken into consideration of TOF, while all metal are considered for other structures.

Fig. 3a shows the volume of H_2 generated using different catalysts, and also demonstrates the advantage of PEI-GO as a support and the validity of the synergistic effect between two metals. For $Pt_{0.17}Co_{0.83}$ without support, it takes 9 min or more to complete dehydrogenation. GO/$Pt_{0.17}Co_{0.83}$ shows an improved catalytic activity, completing the reaction in about 5 min. This is ascribed to the fact that GO improves the dispersion of the small metal NPs, leading to increased catalytic activity. In the absence of GO, PEI/$Pt_{0.17}Co_{0.83}$ also shows good catalytic activity, but slightly lower than that of PEI-GO/$Pt_{0.17}Co_{0.83}$. To figure out the role of GO and PEI in the catalytic hydrolysis of AB, the recyclability test of PEI/$Pt_{0.17}Co_{0.83}$ is carried out, as shown in **Fig. S2**. The amine groups of PEI molecules can immobilize metal ions, that can tune the size of metal NPs and increases the catalytic activity, but with PEI alone as a support, the recyclability of the catalyst is restricted, due to the aggregation and encapsulation of metal NPs. The role GO plays is important, which can tune the morphology of PEI and metal NPs, achieving increased recyclability and better catalytic activity. The advantage of GO compared with other carbon materials is also shown in **Fig. S4**. Compared with other carbon materials like activated carbon (AC) and multi-wall carbon nanotubes (MWCNT), GO shows better capability in tuning the morphology of PEI and metal NPs. For PEI-GO/$Pt_{0.17}Co_{0.83}$, the reaction ended in about 3 min, implying a threefold increase in catalytic activity with the addition of PEI-GO. Apparently, the uniform distribution of small metal NPs (~ 2.3 nm) on PEI-GO is responsible for this enhancement due to the significantly improved accessible SSAs. In addition, the synergistic effect between Pt and Co could be another key factor for the increased catalytic activity. As shown in **Fig. 3b**, monometallic PEI-GO/Pt and PEI-GO/Co catalysts took ~ 3 min and ~ 5 min to complete the dehydrogenation, respectively, even though their precursor concentrations are 20 times higher than the bimetallic counterparts. The low catalytic activity of a physical mixture of PEI-GO/Pt and PEI-GO/Co also verify the existence of the synergistic effect between Pt and Co as shown in **Fig. S5**.

To determine the optimal ratio of Pt/Co for PEI-GO/Pt_xCo_{1-x}, a series of composite catalysts with a constant Pt content were prepared. Clearly, their catalytic activities show a volcano-shape change with increasing Pt/Co ratios, as shown in **Fig. 3c**, **d**, and reach the highest value at a Pt/Co ratio of 0.2. Further increasing Co content ([Co]) leads to a sharp decrease in activity. We suppose that when [Co] is low, the synergistic effect could not be a dominating factor. With the increase of [Co], the synergistic effect gradually becomes dominant and thereby the catalytic activity is greatly improved. With the Pt/Co ratio going beyond 0.2, a large amount of Co NPs form in the vicinity of Pt NPs and even probably result in the occurrence of some core-shell-like structure. This will block active surface sites of Pt NPs and decrease catalytic activity due to the lower activity of Co compared to Pt.[43]

Among our catalysts, PEI-GO/$Pt_{0.17}Co_{0.83}$ exhibits the highest catalytic activity for AB dehydrogenation, with a TOF value of 377.83 mol_{H2} min^{-1} mol^{-1}_{metal} and a H_2 generation rate of 111.28 L_{H2} min^{-1} g^{-1}_{metal}. This is an extremely high catalytic activity and may fulfill the application requirements in fuel cells and portable devices. Compared with other reported noble metal-based catalysts **(**see **Table 1)**, our catalyst reveals the highest catalytic activity among Pt-based bimetallic catalysts, to

the best of our knowledge. We believe that this extraordinary performance would originate from the synergistic effect between Pt and Co NPs and the small size effect of NPs. Next, we choose PEI-GO/$Pt_{0.17}Co_{0.83}$ to evaluate the kinetic, activation energy and recyclability of this class of catalysts.

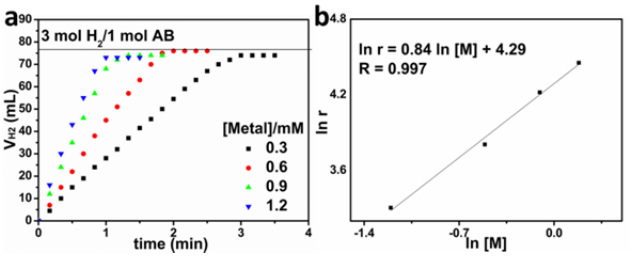

Fig. 4 (a) The hydrolysis of AB at different metal concentrations of PEI-GO/$Pt_{0.17}Co_{0.83}$ at 25 ± 0.5 °C, [AB] = 110 mM and (b) the corresponding plot of H_2 generation rate (ln (r)) versus ln ([metal]). Volume of the dispersion is 10 mL.

The kinetic study of AB hydrolysis can provide valuable information on what experimental factors control the rate of hydrogen generation. The effect of the metal amount on the hydrogen generation rate was investigated by the hydrolysis of 110 mM AB solution at 25 °C with varying metal concentrations (0.3, 0.6, 0.9 and 1.2 mM) while keeping other factors constant. The corresponding results are presented in **Fig. 4a.** The hydrogen generation rate r for different metal amounts of catalysts was calculated from the linear part of each curve. For clarity, a plot of ln (r) *versus* ln ([M]) is re-plotted in **Fig. 4b**. It is seen that ln (r) changes almost linearly with ln ([M]), and the slope obtained is 0.84, suggesting that the PEI-GO/$Pt_{0.17}Co_{0.83}$ catalyzed AB hydrolysis is nearly a first-order reaction with respect to the metal concentration. This is consisted with previous reports,[44] indicating the hydrogen generation rate is controlled by the surface reaction. Therefore, given that the apparent kinetic rate constant is proportional to the total surface area of all metal NPs,[45] the increased active sites on small metal NPs (~ 2.3 nm) are expected to reveal better catalytic performance for hydrolysis dehydrogenation of AB.

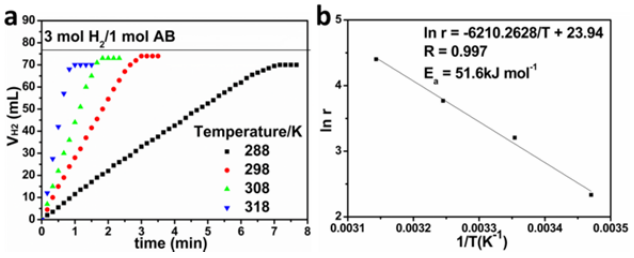

Fig. 5 (a) The hydrolysis of AB catalyzed by PEI-GO/$Pt_{0.17}Co_{0.83}$ at different temperatures with [AB]/[metal] = 366.7, and (b) the corresponding plots of ln r versus the reciprocal absolute temperature 1/T. Volume of the dispersion is 10 mL.

To study the effect of temperature on AB hydrolysis, a series of AB hydrolysis experiments were carried out in the temperature range of 15-45 °C. As shown in **Fig. 5a,** it is found that the hydrogen generation rate rapidly increases with the increase of temperature from 15 to 45 °C. ln (r) *versus* 1/T is re-plotted in **Fig. 5b**, which gives an apparent activation energy of 51.6 kJ mol^{-1} according to the Arrhenius formula. This value is much lower than those of monometallic catalysts (*e.g.*, 62 kJ mol^{-1} for Co/γ-Al_2O_3[46] and 56 kJ mol^{-1} for Pd/zeolite[47]) and bimetallic catalysts (*e.g.*, 52.7 kJ mol^{-1} for Ni-Ru nano-composites[48]), but still higher than other catalysts reported, as listed in **Table 1**. This implies that our catalysts may work much better at high temperatures, which is important for those applications in portable devices and fuel cells that often require medium operation temperatures.

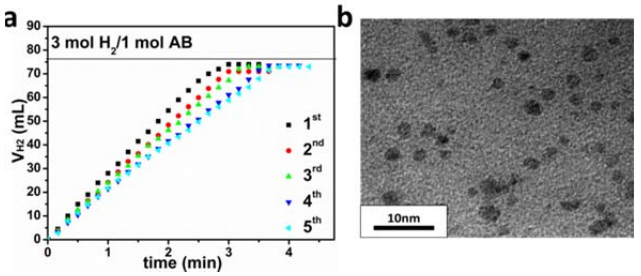

Fig. 6 (a) Hydrogen generation from the hydrolysis of AB catalyzed by PEI-GO/$Pt_{0.17}Co_{0.83}$ at sequential runs at 25 ± 0.5 °C with [AB]/[metal] = 366.7, and (b) TEM image of PEI-GO/$Pt_{0.17}Co_{0.83}$ after 5 cycles. Volume of the dispersion is 10 mL.

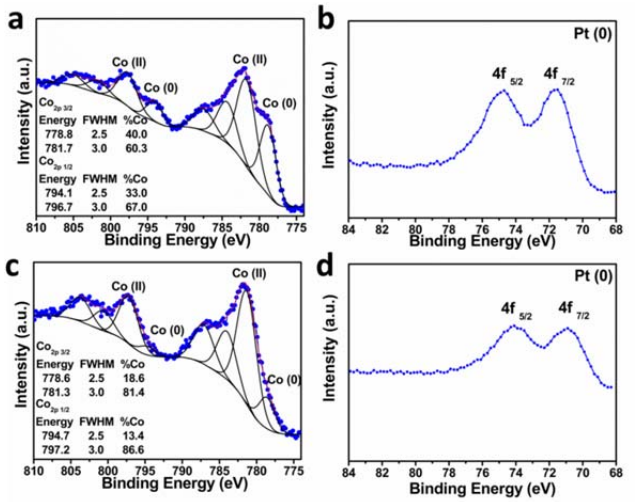

Fig. 7 XPS spectra of Co_{2p} and Pt_{4f} (a, b) before and (c, d) after the catalytic hydrolysis of AB.

As a catalyst of AB hydrolysis, excellent stability and recyclability are important. **Fig. 6a** shows the catalytic activity of PEI-GO/$Pt_{0.17}Co_{0.83}$ after several cycles. It is observed that the hydrogen productivity almost keep constant at 3 mol H_2 per mol AB, but the completion time gradually increases with increasing cycles, indicating the decreased catalytic activity. After the fifth cycle, the PEI-GO/$Pt_{0.17}Co_{0.83}$ still retains ~ 80% of the initial catalytic activity. **Fig. 6b** shows the dispersion of metal NPs after the fifth cycle. The metal NPs do not reveal significant change in size and shape, implying that the reduced activity was not due to the aggregation of metal NPs. XRD patterns of PEI-GO/$Pt_{0.17}Co_{0.83}$ also show that there is no reaction-induced crystalline appears during the cycling catalytic reaction, indicating the stable dispersion of metal NPs (**Fig. S6**). To identify the valence state of Co and Pt in the catalyst, we also conducted the XPS study of PEI-GO/$Pt_{0.17}Co_{0.83}$ before and after the catalytic hydrolysis of AB, shown in **Fig. 7**. More than half of the Co has been oxidized before catalytic reaction due to

the exposure to air during the preparation of XPS sample (**Fig. 7a**). According to **Fig. 7c**, the content of oxidized Co increases from 60% to ~ 80% after the catalytic reaction, indicating the occurrence of Co oxidation during the AB hydrolysis.[49] In **Fig. 7b**, the peaks of zero valent Pt emerge at 71.5 eV and 74.7 eV for Pt $4f_{7/2}$ and $4f_{5/2}$. After the catalytic reaction, the peaks slightly shift to 70.9 eV and 74.1 eV (**Fig. 7d**), which is more close to that of monometallic Pt (70.9 eV for $4f_{7/2}$ and 75.1 eV for $4f_{5/2}$).[50] It may arise from the oxidation of Co and the mitigated synergistic effect between Pt and Co.[21] However, Pt remains to be zero valence state after the catalytic reaction. These results indicate that during the catalytic reaction, Pt is stable, but Co is partially oxidized. Therefore, the decreased catalytic activity during the catalytic reaction would be caused mainly by the oxidation of Co, following the weakened synergistic effect between Pt and Co. For PEI-GO/$Pt_{0.17}Co_{0.83}$, although its activity slightly reduces after several cycles, but it still exhibit a high catalytic activity even after several cycles. This makes it suitable for many practical applications.

Conclusions

We demonstrate the validity of PEI-GO-supported Pt_xCo_{1-x} composite catalysts for the hydrolytic dehydrogenation of AB. The PEI adsorbed on GO facilitated the size control and uniform dispersion of metal NPs. Owing to the anchoring effect of PEI to precursor metal ions, the resulting metal NPs revealed a small particle size, 2.3 nm. By tuning the molar ratio of Pt/Co precursors, we synthesized a series of PEI-GO/Pt_xCo_{1-x} composite catalysts, among which PEI-GO/$Pt_{0.17}Co_{0.83}$ exhibited extraordinary catalytic activity compared to their monometallic counterparts. We propose that two key factors are responsible for the improved activity; that is, the synergistic effect between two metals and small particle sizes (high SSA) of metal NPs. We observed a volcano-shape relationship with varying Pt/Co ratios, as well as a sharp decrease in catalytic activity after [Pt]/[Co] going beyond 0.2, which suggests the significant dependence of the synergistic effect on the component of bimetallic catalysts. In the catalytic kinetics of AB hydrolysis, a first-order reaction kinetics is believed to originate from large specific surface areas of bimetallic NPs, given that the apparent kinetic rate constant is strictly proportional to the total surface areas of all metal NPs. Our results show that PEI-GO/$Pt_{0.17}Co_{0.83}$ exhibits an unprecedented TOF value (377.83 mol_{H2} min^{-1} mol^{-1}_{metal}), a high hydrogen generation rate (111.28 L_{H2} min^{-1} g^{-1}_{metal}) and a moderate activation energy (51.6 kJ mol^{-1}). These properties make this novel catalyst highly competitive compared to all other noble metal based bimetallic catalysts. Also, we revealed that the PEI-GO/$Pt_{0.17}Co_{0.83}$ catalyst has good magnetic recyclability and retained ~80% of the initial activity after 5 cycles and no significant morphology change was observed. As a result, we believe that the high efficiency, low cost advantages of PEI-GO/Pt_xCo_{1-x} will open an attractive approach for many practical applications such as portable devices and fuel cells.

Acknowledgements

We thank Ms. Limin Sun and Ms. Qianqian Hu (Shanghai Jiao Tong Univ.) for her assistance with XPS. This work was supported by National Basic Research Program of China (grant no. 2011CB605702), NSF of China (grant no. 50573014, 50773012 and 51173027), and Shanghai Nanotechnology Program (grant no. 1052nm00400).

Notes and references

[a] State Key Laboratory of Molecular Engineering of Polymers, and Department of Macromolecular Science, Fudan University, 220 Handan Road, Shanghai, 200433, China. Tel/Fax: 86-21-5566 4589; Email: hongbinlu@fudan.edu.cn.

† These authors contributed equally to the work.

1 R. J. Keaton, J. M. Blacquiere, and R. T. Baker, *J. Am. Chem. Soc.*, 2007, **129**, 1844-1845.
2 S. C. Amendola, S. L. Sharp-Goldman, M. S. Janjua, M. T. Kelly, P. J. Petillo and M. Binder, *J. Power Sources*, 2000, **85**, 186-189.
3 Y. Kojima, Y. Kawai, H. Nakanishi and S. Matsumoto, *J. Power Sources*, 2004, **135**, 36-41.
4 G. A. Deluga, J. R. Salge, L. D. Schmidt and X. E. Verykios, *Science*, 2004, **303**, 993-997.
5 X. B. Chen, S. H. Shen, L. J. Guo and S. S. Mao, *Chem. Rev.*, 2010, **110**, 6503-6570.
6 C. W. Hamilton, R. T. Baker, A. Staubitz and I. Manners, *Chem. Soc. Rev.*, 2009, **38**, 279-293.
7 U. B. Demirci and P. Miele, *Energy Environ. Sci.*, 2009, **2**, 627-637.
8 F. H. Stephens, V. Pons and R. T. Baker, *Dalton Trans.*, 2007, 2613-2626.
9 G. Wolf, J. Baumann, F. Baitalow and F. P. Hoffmann, *Thermochimica Acta*, 2000, **343**, 19-25.
10 M. Chandra and Q. Xu, *J. Power Sources*, 2006, **156**, 190-194.
11 S. Akbayrak, S. Gençtürk, İ. Morkan and S. Özkar, *RSC Adv.*, 2014, **4**, 13742-13748.
12 S. S. Mal, F. H. Stephens and R. T. Baker, *Chem. Commun.*, 2011, **47**, 2922-2924.
13 F. Y. Qiu, Y. L. Dai, L. Li, C. C. Xu, Y. N. Huang, C. C. Chen, Y. J. Wang, L. F. Jiao and H. T. Yuan, *Int. J. Hydrogen Energy*, 2014, **39**, 436-441.
14 Y. W. Yang, Z. H. Lu, Y. J. Hu, Z. J. Zhang, W. M. Shi, X. S. Chen and T. T. Wang, *RSC Adv.*, 2014, **4**, 13749-13752.
15 J. M. Yan, X. B. Zhang, S. Han, H. Shioyama and Q. Xu, *Inorg. Chem.*, 2009, **48**, 7389-7393.
16 A. K. Singh and Q. Xu, *ChemCatChem*, 2013, **5**, 652-676.
17 L. Yang, J. Su, X. Y. Meng, W. Luo and G. Z. Cheng, *J. Mater. Chem. A*, 2013, **1**, 10016-10023.
18 F. Tao, *Chem. Soc. Rev.*, 2012, **41**, 7977-7979.
19 D. H. Sun, V. Mazumder, Ö. Metin and S. H. Sun, *ACS Nano*, 2011, **5**, 6458-6464.
20 H. L. Jiang, T. Umegaki, T. Akita, X. B. Zhang, M. Haruta and Q. Xu, *Chem. Eur. J.*, 2010, **16**, 3132-3137.
21 M. Wen, S. Q. Zhou, Q. S. Wu, J. Y. Zhang, Q. N. Wu, C. X. Wang and Y. Z. Sun, *J. Power Sources*, 2013, **232**, 86-92.
22 A. J. Amali, K. Aranishi, T. Uchida and Q. Xu, *Part. Part. Syst. Charact.*, 2013, **30**, 888-892.
23 S. Garaj, W. Hubbard, A. Reina, J. Kong, D. Branton and J. A. Golovchenko, *Nature*, 2010, **467**, 190-193.
24 K. S. Novoselov, A. K. Geim, S. V. Morozov, D. Jiang, Y. Zhang, S. V. Dubonos, I. V. Grigorieva and A. A. Firsov, *Science*, 2004, **306**, 666-669.
25 N. Cao, J. Su, W. Luo and G. Z. Cheng, *Int. J. Hydrogen Energy*, 2014, **39**, 426-435.
26 P. Yang, S. Y. Jin, Q. Z. Xu and S. H. Yu, *Small*, 2013, **9**, 199-204.

27 F. Y. Qiu, L. Li, G. Liu, Y. J. Wang, C. H. An, C. C. Xu, Y. N. Xu, Y. Wang, L. F. Jiao and H. T. Yuan, *Int. J. Hydrogen Energy*, 2013, **38**, 7291-7297.
28 M. Fang, Z. X. Chen, S. Z. Wang and H. B. Lu, *Nanotechnology*, 2012, **23**, 085704.
29 H. Bai, C. Li and G. Q. Shi, *Adv. Mater.*, 2011, **23**, 1089-1115.
30 G. Goncalves, P. A. A. P. Marques, C. M. Granadeiro, H. I. S. Nogueira, M. K. Singh and J. Grácio, *Chem. Mater.*, 2009, **21**, 4796-4802.
31 X. H. Zhou, Z. X. Chen, D. H. Yan and H. B. Lu, *J. Mater. Chem.*, 2012, **22**, 13506-13516.
32 Y. Zhang, B. Chen, L. M. Zhang, J. Huang, F. H. Chen, Z. P. Yang, J. L. Yao and Z. J. Zhang, *Nanoscale*, 2011, **3**, 1446-1450.
33 Y. Zhang, B. Chen, L. Zhang, J. Huang, F. Chen, Z. Yang, J. Yao and Z. Zhang. *Nanoscale*, 2011, **3**, 1446-1450.
34 X. J. Yang, F. Y. Cheng, J. Liang, Z. L. Tao and J. Chen, *Int. J. Hydrogen Energy*, 2011, **36**, 1984-1990.
35 X. J. Yang, F. Y. Cheng, Z. L. Tao and J. Chen, *J. Power Sources*, 2011, **196**, 2785-2789.
36 X. Wang, D. P. Liu, S. Y. Song and H. J. Zhang, *Chem. Eur. J.*, 2013, **19**, 8082-8086.
37 J. Wang, Y. L. Qin, X. Liu and X. B. Zhang, *J. Mater. Chem.*, 2012, **22**, 12468-12470.
38 M. Wen, Q. N. Wu, J. Peng, Q. S. Wu and C. X. Wang, *J. Colloid Interf. Sci.*, 2014, **416**, 220-226.
39 X. J. Yang, F. Y. Cheng, J. Liang, Z. L. Tao and J. Chen, *Int. J. Hydrogen Energy*, 2009, **34**, 8785-8791.
40 G. P. Rachiero, U. B. Demirci and P. Miele, *Int. J. Hydrogen Energy*, 2011, **36**, 7051-7065.
41 M. Chandra and Q. Xu, *J. Power Sources*, 2007, **168**, 135-142.
42 A. Aijaz, A. Karkamkar, Y. J. Choi, N. Tsumori, E. Rönnebro, T. Autrey, H. Shioyama and Q. Xu, *J. Am. Chem. Soc.*, 2012, **134**, 13926-13929.
43 G. Z. Chen, S. Desinan, R. Rosei, F. Rosei and D. L. Ma, *Chem. Eur. J.*, 2012, **18**, 7925-7930.
44 Ö. Metin and S. Özkar, *Int. J. Hydrogen Energy.*, 2011, **36**, 1424-1432.
45 C. Z. Zhu, P. Wang, L. Wang, L. Han and S. J. Dong, *Nanoscale*, 2011, **3**, 4376-4382.
46 Q. Xu and M. Chandra, *J. Alloy. Compd.*, 2007, **446-447**, 729-732.
47 M. Rakap and S. Özkar, *Int. J. Hydrogen Energy*, 2010, **35**, 1305-1312.
48 S. C. Amendola, S. L. Sharp-Goldman, M. S. Janjua, N. C. Spencer, M. T. Kelly, P. J. Petillo and M. Binder, *Int. J. Hydrogen Energy*, 2000, **25**, 969-975.
49 U. B. Demirci and P. Miele, *Phys. Chem. Chem. Phys.*, 2010, **12**, 14651-14665.
50 B. V. Crist, On-Screen PDF Handbook of Monochromatic XPS spectra, In: The Elements and Native Oxides, vol. 1, XPS International, Inc, 1999.